Cellular and Molecular Life Sciences (2019) 76:193–207
https://doi.org/10.1007/s00018-018-2942-5

ORIGINAL ARTICLE

DYRK1B regulates Hedgehog-induced microtubule acetylation

Rajeev Singh[1] · Philipp Simon Holz[1] · Katrin Roth[2] · Anna Hupfer[1] · Wolfgang Meissner[1] · Rolf Müller[1] · Malte Buchholz[3] · Thomas M. Gress[3] · Hans-Peter Elsässer[4] · Ralf Jacob[4] · Matthias Lauth[1]

Received: 12 April 2018 / Revised: 25 September 2018 / Accepted: 8 October 2018 / Published online: 13 October 2018

Abstract

The posttranslational modification (PTM) of tubulin subunits is important for the physiological functions of the microtubule (MT) cytoskeleton. Although major advances have been made in the identification of enzymes carrying out MT-PTMs, little knowledge is available on how intercellular signaling molecules and their associated pathways regulate MT-PTM-dependent processes inside signal-receiving cells. Here we show that Hedgehog (Hh) signaling, a paradigmatic intercellular signaling system, affects the MT acetylation state in mammalian cells. Mechanistically, Hh pathway activity increases the levels of the MT-associated DYRK1B kinase, resulting in the inhibition of GSK3β through phosphorylation of Serine 9 and the subsequent suppression of HDAC6 enzyme activity. Since HDAC6 represents a major tubulin deacetylase, its inhibition increases the levels of acetylated MTs. Through the activation of DYRK1B, Hh signaling facilitates MT-dependent processes such as intracellular mitochondrial transport, mesenchymal cell polarization or directed cell migration. Taken together, we provide evidence that intercellular communication through Hh signals can regulate the MT cytoskeleton and contribute to MT-dependent processes by affecting the level of tubulin acetylation.

Keywords Hedgehog · SHH · DYRK1B · HDAC6 · GSK3β · Microtubules · Acetylation · Organelle transport · Cell migration

Abbreviations

DYRK1B	Dual specificity-regulated kinase 1B (a.k.a. MIRK)
Hh	Hedgehog
SHH	Sonic Hedgehog
GLI1	Glioma-associated oncogene 1
GSK3β	Glycogen synthase kinase 3 beta
HDAC6	Histone deacetylase 6
MT	Microtubule
AcTub	Acetylated α-tubulin
SAG	Smoothened agonist
SANT	Smoothened antagonist
MTOC	Microtubule (MT) organizing center

Introduction

The microtubule (MT) cytoskeleton is crucial for a vast number of cellular processes including signal transduction, organelle transport, mitosis and cell migration. A major mode of MT regulation is through posttranslational modification (PTM) such as acetylation, phosphorylation, polyglycylation, polyglutamylation and others [34, 48, 80]. One of the best-studied modifications is acetylation, which can occur on Lys40 of the α-subunit of the α/β heterodimer within MTs [35]. Acetylated α-tubulin (AcTub) is often associated with stable and long-lived MTs, such as those observed, e.g., in primary cilia. Although initial speculations about tubulin PTMs affecting transport velocity along MTs were questioned later, these modifications seem to determine the

Electronic supplementary material The online version of this article (https://doi.org/10.1007/s00018-018-2942-5) contains supplementary material, which is available to authorized users.

✉ Matthias Lauth
lauth@imt.uni-marburg.de

[1] Institute of Molecular Biology and Tumor Research (IMT), Center for Tumor- and Immune Biology (ZTI), Philipps University, Hans-Meerwein-Str. 3, 35043 Marburg, Germany

[2] Imaging Core Facility, Center for Tumor- and Immune Biology (ZTI), Philipps University, Hans-Meerwein-Str. 3, 35043 Marburg, Germany

[3] Clinic for Gastroenterology, Endocrinology, Metabolism and Infectiology, Philipps University, Marburg, Germany

[4] Institute of Cytobiology and Cytopathology, Philipps University, Robert Koch Str. 6, 35037 Marburg, Germany

binding specificity of selected motor proteins and thereby facilitate the transport of certain cargoes along MT tracks [10, 30, 61, 78]. Indeed, increasing tubulin acetylation has been shown to promote MT-directed mitochondrial transport in neurons [13] and to compensate for vesicular transport deficits in a cellular model of Huntington's disease [21]. Moreover, recent data show that acetylation protects MTs from mechanical breakage, which might affect transport processes indirectly [58, 81].

Key enzymes regulating MT acetylation are α-tubulin acetyl transferase (ATAT, a.k.a. αTAT1 or MEC17) and histone deacetylase 6 (HDAC6), which add or remove acetyl groups from α-tubulin, respectively [2, 32, 53]. HDAC6 is a multifunctional protein with sequence homology to nuclear HDACs, deacetylating many non-histone proteins such as tubulin [46]. It is involved in a wide variety of cellular processes including signal transduction [18, 20, 49, 70], aggresome formation [8, 37], stress granule biology [40] and gene transcription [12].

Although a lot of information about the enzymes governing tubulin PTMs has been gathered in recent years, comparatively little knowledge is available about how this cytoskeletal regulation is controlled by signaling networks. This information would be of particular interest as signaling pathways are perfectly suited to sense extracellular conditions and to translate these cues into modifications of the intracellular cytoskeleton.

One example of such a signaling system is the evolutionary conserved Hedgehog (Hh) pathway. Hedgehog signaling is absolutely essential for proper embryonic development [9, 50] and its overactivation is associated with numerous forms of cancer [5, 44, 55]. In many instances, during development, tissue repair or cancer, Hh ligands (Sonic Hh (SHH), Desert Hh (DHH), Indian Hh (IHH)) signal from epithelial to neighboring mesenchymal cell types [65, 71]. Binding to the primary cilia-localized Patched1 (PTCH1) receptor releases Smoothened (SMO) from PTCH1-mediated inhibition and allows for the activation of the GLI family of transcription factors (GLI1, GLI2, GLI3) [1, 27, 33, 63, 64]. While Hh signaling has been shown to affect the actin cytoskeleton [6, 56, 57, 67], very little is known about its effects on the MT network. It is well appreciated that MTs and MT-associated transport proteins regulate Hh signaling, mostly through their crucial roles in primary cilia [15, 39, 62], but how Hh impacts on MTs is less studied [42].

In this work, we show that activated Hh signaling promotes the acetylation of microtubules and contributes to AcTub-dependent processes such as cell polarization, migration or organelle transport. Mechanistically, we identify the Hh-regulated DYRK1B kinase as a negative modulator of GSK3β, leading to the suppression of HDAC6 enzyme activity and an increase in tubulin acetylation. Using biochemical assays as well as super-resolution microscopy, we could further show that DYRK1B, GSK3β and HDAC6 are associated to MTs. In summary, using Hh signaling as a paradigm, we describe a mechanistic framework how intercellular communication can impinge on cytoskeletal regulation and cell function.

Results

Hedgehog signaling regulates tubulin acetylation

In line with a previous report [42], we found that Hh signaling promotes the increase of α-tubulin acetylation in fibroblasts, a cell type representing a major Hh-responsive cell population in vivo. When NIH3T3 cells, cultured under low serum conditions, were treated with the Hh pathway-activating synthetic compound SAG (Smoothened agonist) [11], we observed an induction of acetylated tubulin (AcTub) in immunofluorescence (Fig. 1a, b) and in Western blotting experiments (Fig. 1c, d). This AcTub increase positively correlated with the induction of the Hh pathway target Gli1 and the levels of the dual-specificity tyrosine (Y)-regulated kinase 1B (Dyrk1b, a.k.a. as Mirk) [51] which we have previously shown to be upregulated by Hh signaling [72] (Fig. 1c, d). However, *Dyrk1b* mRNA levels were not significantly affected by Hh signaling in these cells, as were the levels of AcTub regulating enzymes such as *Hdac6* and *Mec17* (*αTat1*) (Fig. S1A), arguing for a posttranscriptional regulation of Dyrk1b by Hh.

Furthermore, Hh-induced tubulin acetylation and Dyrk1b induction was also observed in other fibroblast cells such as in SAG-treated mouse embryonic fibroblasts (MEFs) (Fig. 1e), demonstrating that this effect was not restricted to NIH3T3 cells. To rule out a Hh-unrelated effect of the compound SAG, we investigated MEF cells stably expressing SHH ligand ($MEF^{[SHH]}$ cells [47]) and found that pathway inhibition with the SMO inhibitor SANT [11] concomitantly reduced the levels of AcTub and Dyrk1b (Fig. 1f). Based on these experiments, we hypothesized that Dyrk1b could be involved in mediating all or some of the effects of Hh on AcTub.

To demonstrate that the Hh-induced AcTub increase was indeed mediated through Dyrk1b, we knocked down endogenous *Dyrk1b* by means of RNAi in MEF cells. As can be seen in Fig. 1g (and Fig. S1B), the SAG-mediated increase in acetylated tubulin could be fully blocked upon depletion of Dyrk1b. In support of our finding of Hh-regulated tubulin acetylation, the elevated AcTub levels previously seen in $MEF^{[SHH]}$ cells could be reduced by siRNA transfection targeting *Dyrk1b* (Fig. 1h). These experiments suggest that Hh signaling increases Dyrk1b protein levels by post-transcriptional mechanisms leading to a rise in Dyrk1b-mediated tubulin acetylation.

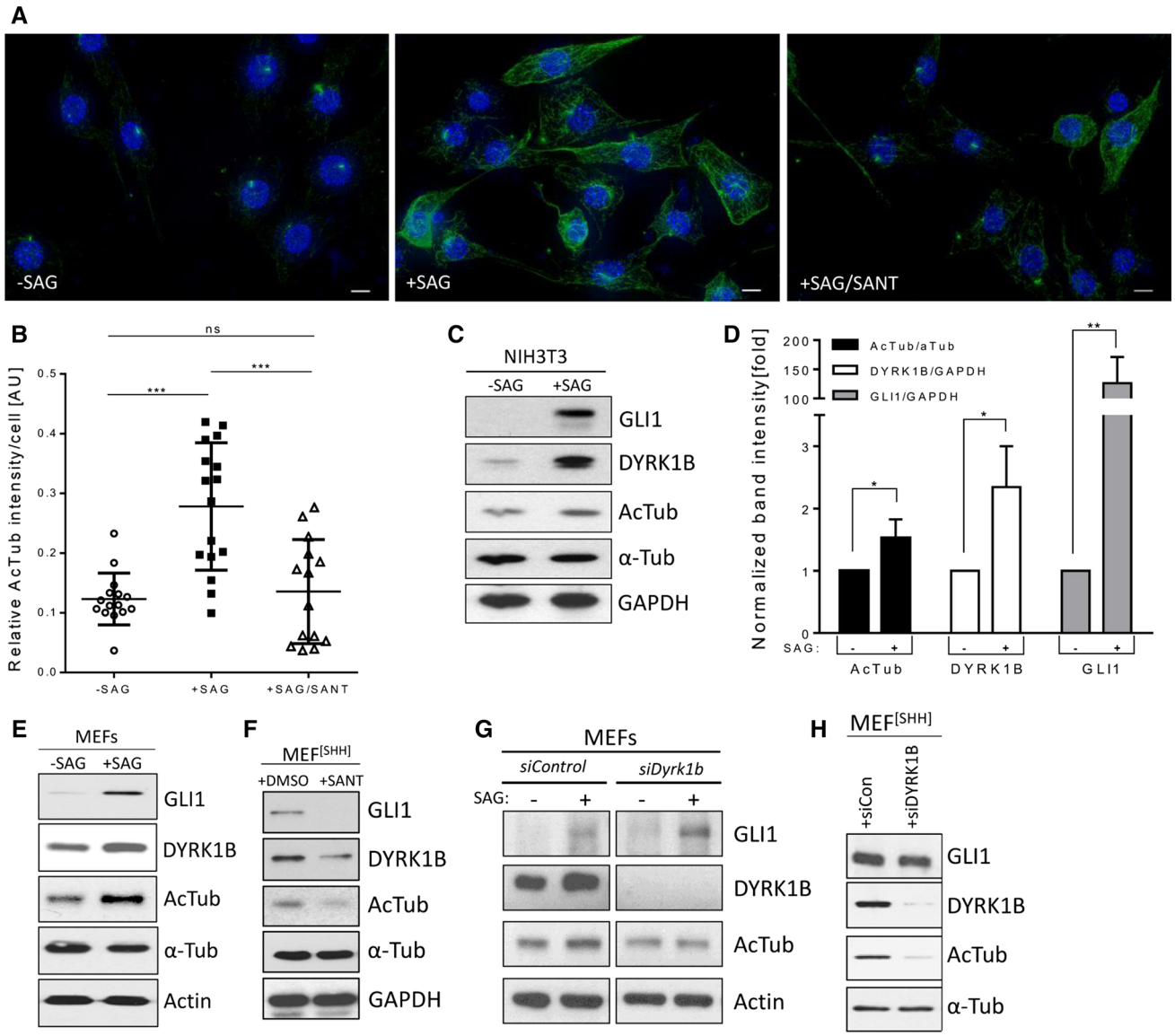

Fig. 1 Hh signaling increases levels of DYRK1B and tubulin acetylation. **a** Immunofluorescent AcTub (green) staining of NIH3T3 cells treated with either DMSO, smoothened agonist SAG (100 nM) or SAG plus SANT1 (200 nM). Scale bars equals 10 µm. Blue = DAPI staining. **b** Quantification of AcTub intensities as shown in **a**. Plotted is the AcTub fluorescence intensity per cell measured in 14–16 different viewing fields from three independent experiments. In total, at least 220 cells were analyzed per condition. **c** Western blot of NIH3T3 cell lysates treated with SAG. Shown is a representative blot of three. **d** Quantification of (C) (mean of $n = 3 \pm$ SD). Values were normalized to GAPDH levels or total α-Tubulin (aTub). **e** Western blot of MEF lysates treated with SAG (100 nM, 48–72 h). Shown is one blot of two. **f** Western blot of MEF cell lysates stably expressing SHH (MEF$^{[SHH]}$ cells). Cells were treated with the SMO antagonist SANT to block Hh signaling. Shown is a representative blot of three. **g** Western blot of MEF cell lysates transfected with control siRNA or with *Dyrk1b*-specific siRNA. Cells were treated with SAG (100 nM, 48 h). Shown is one blot of two. **h** Western blot depicting the changes in AcTub levels after RNAi-mediated knock-down of *Dyrk1b* in MEF$^{[SHH]}$ cells. Shown is one blot of two independent experiments

The expression of DYRK1B is sufficient for AcTub induction

Given the cross-talk between Hh signaling and tubulin acetylation, we were interested to address the role of DYRK1B in more detail. To this end, we generated NIH3T3 cells stably expressing a V5-tagged form of this kinase (NIH3T3$^{[DYRK1B]}$ cells). Intriguingly, these cells displayed a strikingly different morphology in culture when compared to control cells (Fig. 2a). While control cells (NIH3T3$^{[Mock]}$) possessed the expected elongated, spindle-shaped morphology of mesenchymal cells, the *DYRK1B*-overexpressing cells had much smaller and rounder cell bodies with longer cellular extensions, suggesting a potential cytoskeletal effect induced by the increased *DYRK1B* expression. Indeed, when analyzing the levels of AcTub in these cells, we found strikingly

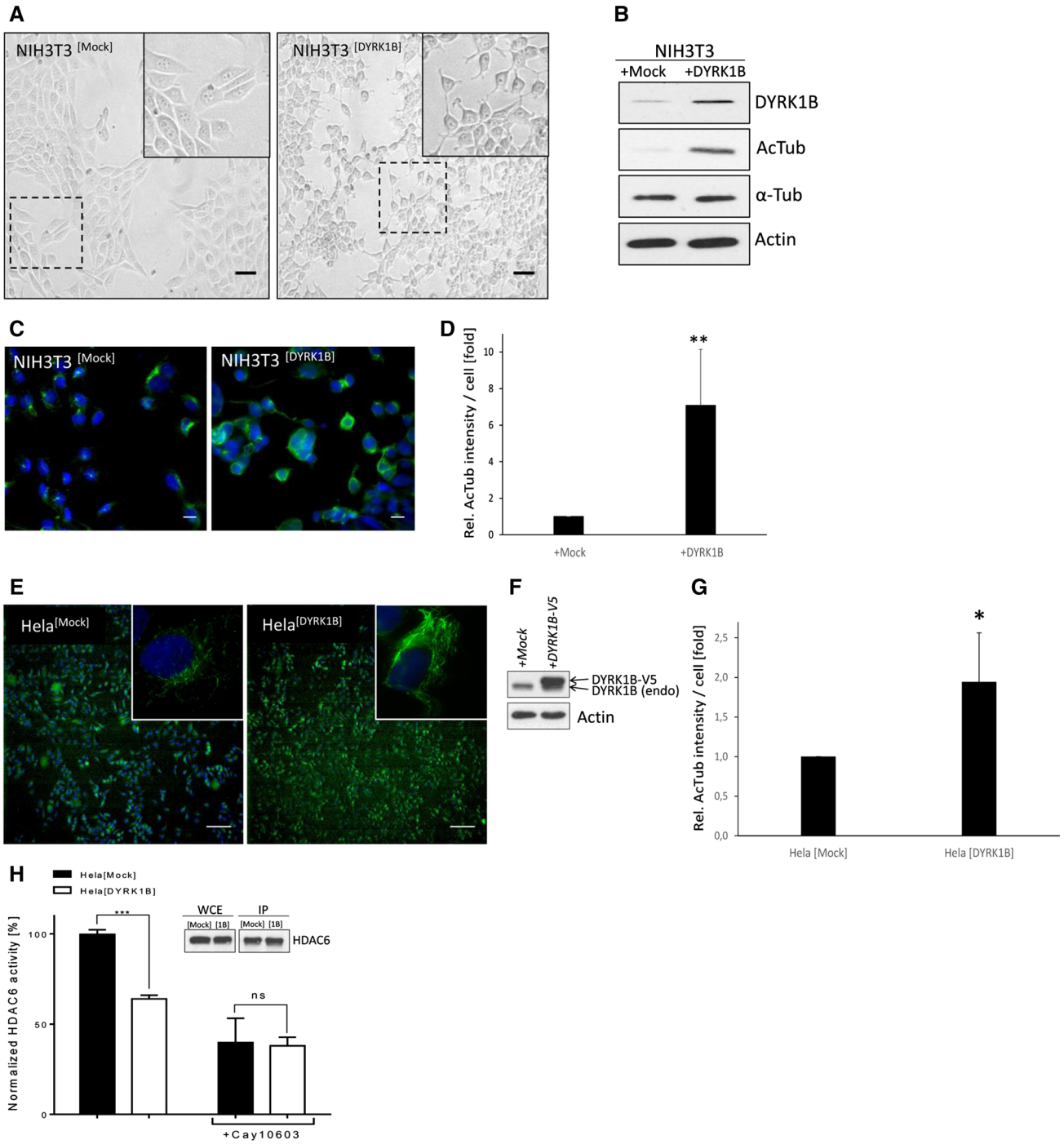

Fig. 2 DYRK1B expression is sufficient to augment tubulin acetylation. **a** Bright field images of NIH3T3 cells stably expressing mock control (empty vector) or *DYRK1B*. Scale bar 50 µm. **b** Western blot of NIH3T3 cells stably expressing DYRK1B or empty vector control (mock) showing the expression levels of the indicated proteins. Shown is one representative blot of four. **c** AcTub immunofluorescence image (green) of control NIH3T3 (mock) or of cells with stable DYRK1B expression. **d** Quantification of the results obtained in **c**. Shown is the mean of $n = 5 \pm$ SD. AcTub = Acetylated α-tubulin. **e** Acetylated tubulin staining (green) in human Hela cells stably expressing *DYRK1B* or empty vector control (mock). Blue = Nuclei. Scale bar 100 µm. **f** Western blot verifying DYRK1B-V5 overexpression of cells depicted in **e**. **g** Quantification of AcTub intensities of cells shown in **e**. Shown is the mean of $n = 4 \pm$ SD. **h** In vitro HDAC6 enzyme assay (mean of $n = 3 \pm$ SD). Endogenous HDAC6 protein was immunoprecipitated from Hela cells stably expressing empty vector control (mock) or *DYRK1B*. HDAC6 activity was subsequently measured with a luminometric HDAC assay. Values were normalized against western blot band intensities of immunoprecipitated HDAC6 (see inset as example). The selective HDAC6 inhibitor Cay10603 (100 nM) was used as a positive control

elevated levels of acetylated tubulin (Fig. 2b–d), showing that the mere overexpression of *DYRK1B* can lead to AcTub induction. Interestingly, we could not observe increased levels of AcTub upon transfection of other DYRK family members such as DYRK1A, DYRK2 or DYRK3 (Fig. S2A). In addition, expression of a kinase-dead DYRK1B mutant was unable to induce tubulin acetylation, suggesting that DYRK1B's kinase activity is required for the effect (Fig. S2B).

Intriguingly, DYRK1B-induced acetylated MTs were more resistant to the depolymerizing activity of Nocodazole (Fig. S2C,D), which is in line with a previous report describing a protective function of DYRK1B against Nocodazole [17]. We furthermore investigated whether an increased *DYRK1B* expression might affect the morphology of primary cilia, a cellular organelle rich in AcTub and essential for proper Hh signal transduction [25, 59]. However, using immunofluorescent staining with an α-detyrosinated tubulin antibody (a primary cilia marker) as well as by electron microscopy, we were unable to detect gross morphological aberrations in the (ultra)structure of primary cilia upon *DYRK1B* overexpression (Fig. S2E).

Next, we went on to investigate whether the finding of increased AcTub levels in *DYRK1B*-expressing cells was specific to fibroblasts. As can be seen in Fig. 2e–g, we could recapitulate these observations also in Hela cells stably transfected with *DYRK1B* (Hela$^{[DYRK1B]}$ cells). Since HDAC6 is known as a major negative determinant of the tubulin acetylation status, we used the Hela$^{[DYRK1B]}$ cells to investigate whether DYRK1B expression would diminish the overall HDAC6 enzyme activity when compared to control cells. We immunoprecipitated endogenous HDAC6 from control and from *DYRK1B*-expressing Hela cell lines and subjected the precipitate to a luminometric in vitro deacetylase assay. Indeed, the HDAC6 enzyme activity (normalized to the amount of total HDAC6 protein precipitated) was significantly lower (by about 40%) in *DYRK1B*-expressing cells. This difference was blunted when a HDAC6-selective inhibitor (Cay10603) was co-applied to the deacetylase assay (Fig. 2h). Taken together, these experiments demonstrate that the increased expression of DYRK1B is sufficient to elicit MT acetylation in the absence of Hh receptor activation. Furthermore, increased DYRK1B levels result in functional downregulation of HDAC6, a known master regulator of MT acetylation.

DYRK1B phosphorylates the inhibitory Ser9 site of GSK3β

In our attempts to decipher the mechanistic link between DYRK1B and HDAC6, we speculated that the DYRK1B kinase might directly phosphorylate HDAC6. To address this issue, we performed in vitro kinase assays with both proteins but failed to observe a direct phosphorylation (not shown), which prompted us to hypothesize an indirect mechanism. One example of such a mechanism would envision that DYRK1B does not phosphorylate HDAC6 directly, but instead phosphorylates one of the several HDAC6-regulating proteins. To this end, we focused on glycogen synthase kinase 3 β (GSK3β), which had previously been shown to regulate HDAC6 in a stimulatory manner [13] and is inhibited by DYRK1A in neurons and adipocytes [73].

Hence, we wanted to find out whether Hh/DYRK1B would inhibit GSK3β, thereby indirectly leading to the suppression of HDAC6 activity. To this end, we first investigated whether Hh signaling modulates Gsk3β. In fact, Western blot analyses of lysates from SAG-treated cells revealed that Hh activity promotes the phosphorylation of Ser9 (Fig. 3a), an important regulatory residue known to control phosphorylation-induced Gsk3β inactivation. In contrast, blocking Hh pathway activity in continuously *SHH*-expressing cells reduced the levels of phospho-Gsk3β^{S9} (Fig. 3b).

Next, we investigated whether Dyrk1b plays a role in Hh-induced Gsk3β phosphorylation and found that RNAi-mediated knock-down of endogenous *Dyrk1b* resulted in a concomitant reduction of phospho-Gsk3β^{S9} levels in MEF$^{[SHH]}$ cells (Fig. 3c) and in SAG-exposed NIH3T3 cells (Fig. S3A). In addition, the pharmacological blockade of Dyrk1b with the selective inhibitor AZ191 [3] reduced phospho-Gsk3β^{S9} and AcTub levels in SAG-treated cells (Fig. 3d) as well as in cells constitutively expressing *SHH* (Fig. S3B). Moreover, the stable expression of *DYRK1B* (in the absence of Hh signaling) was sufficient to induce Gsk3β phosphorylation (Fig. 3e), suggesting a close functional connection between these two players. In agreement with the above findings, transfection of kinase competent, but not of kinase-dead DYRK1B promoted Gsk3β phosphorylation (Fig. S3C). Encouraged by these results, we performed in vitro kinase assays and found that recombinant DYRK1B was able to phosphorylate immunoprecipitated GSK3β on Ser9 under in vitro conditions (Fig. 3f). In line with the idea that phosphorylation on Ser9 renders GSK3β inactive, we could find that pharmacological inhibition of endogenous GSK3β also increased AcTub levels in cells (Fig. S3D). Furthermore, overexpression of a non-phosphorylatable GSK3β mutant (GSK3β^{S9A}) reduced the induction of AcTub by DYRK1B (Fig. S3E and S3F).

In summary, we could provide evidence that Hh signaling, through upregulation of Dyrk1b, inactivates Gsk3β by phosphorylation on the important control residue Ser9. This subsequently inhibits Hdac6 enzyme activity, leading to an increase in cellular AcTub levels.

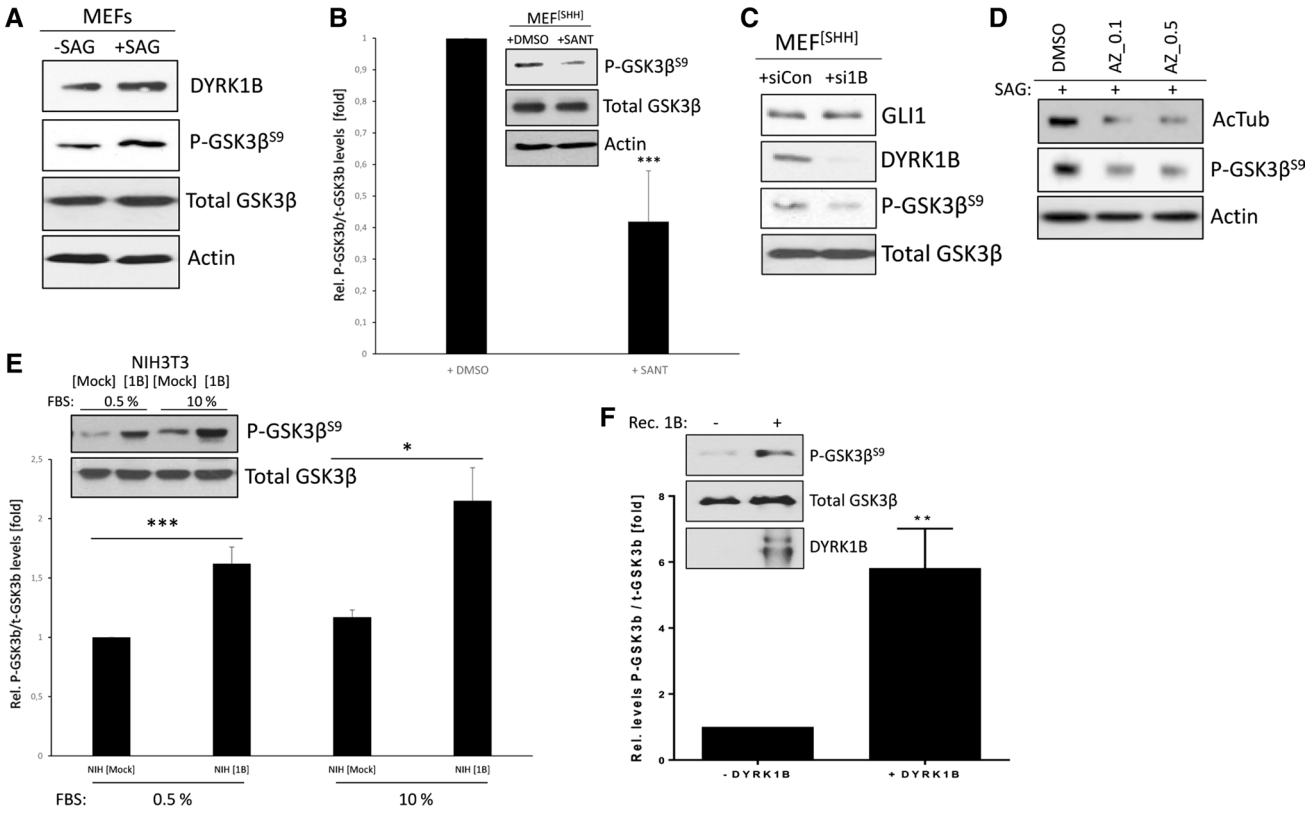

Fig. 3 Hh and DYRK1B inactivate GSK3β by Ser9 phosphorylation. **a** Western blot example of $n=2$ independent experiments showing phospho-Gsk3β^{S9} levels after SAG induction. **b** Western blot data and the corresponding phospho-Gsk3β^{S9} quantification (mean of $n=3\pm$SD) of MEF$^{[SHH]}$ cells treated with the SMO inhibitor SANT (200 nM, 48–72 h). **c** MEF$^{[SHH]}$ cell lysates transfected with control siRNA (siCon) or with *Dyrk1b*-directed siRNA (si1B). Shown is one representative blot of three. **d** Western blot of NIH3T3 lysates. Cells were pre-treated with SAG (100 nM) for 48 h prior to addition of the DYRK1B inhibitor AZ191 (AZ, 0.1 or 0.5 µM) for 3 h. **e** Quantification of Phospho-Gsk3β^{S9} levels in NIH3T3 stably expressing empty vector (mock) or V5-tagged *DYRK1B* in two different serum concentrations (mean of $n=3\pm$SD). Inset: one representative blot. **f** Quantification of in vitro kinase assays with recombinant DYRK1B enzyme and immunoprecipitated GSK3β. Shown is the mean of $n=3\pm$SD. Rec.1B = Recombinant DYRK1B. The inset depicts a representative blot

DYRK1B is associated with the MT cytoskeleton

Since our data suggested that DYRK1B regulates tubulin acetylation and since it was known that HDAC6 and GSK3β are localized to MTs [32, 75, 83, 84], we were interested whether Dyrk1b would also be associated to MTs. To analyze this issue in more depth, we performed biochemical MT-association assays (MTaa) using control or SAG-treated NIH3T3 cells to purify protein fractions bound to polymerized MTs. As can be seen in Fig. 4a, a fraction of total Dyrk1b (as well as Gsk3β which was included as positive control) could consistently be found in the pelleted fraction ('MT') containing polymerized MTs. Stimulation with the SMO agonist SAG led to increased levels of MT-bound Dyrk1b, which was, however, most likely the result of an overall increase in protein amount and not due to a specific recruitment to MTs.

To support the MT-localization of DYRK1B by an independent technical approach, we performed sub-diffraction super-resolution microscopy (GSD-ground state depletion microscopy) and were able to visualize transfected V5-tagged DYRK1B on endogenous MTs (Fig. 4b) in human fibroblasts (PSC). As shown in figure S4A, DYRK1B also regulates AcTub levels in these cells. In addition, super-resolution microscopy also revealed the localization of endogenous DYRK1B on single MT tracks in Hela cells (which were used here since the endogenous DYRK1B levels in PSC cells were difficult to visualize by microscopy) (Fig. 4c). As a positive control of another protein previously reported to be MT-associated, we were able to detect endogenous HDAC6 on defined MT tracks in PSC fibroblasts (Fig. 4d). Taken together, using biochemical as well as microscopic techniques we could provide evidence for DYRK1B being associated with MTs, the expected subcellular localization for a MT-regulating protein.

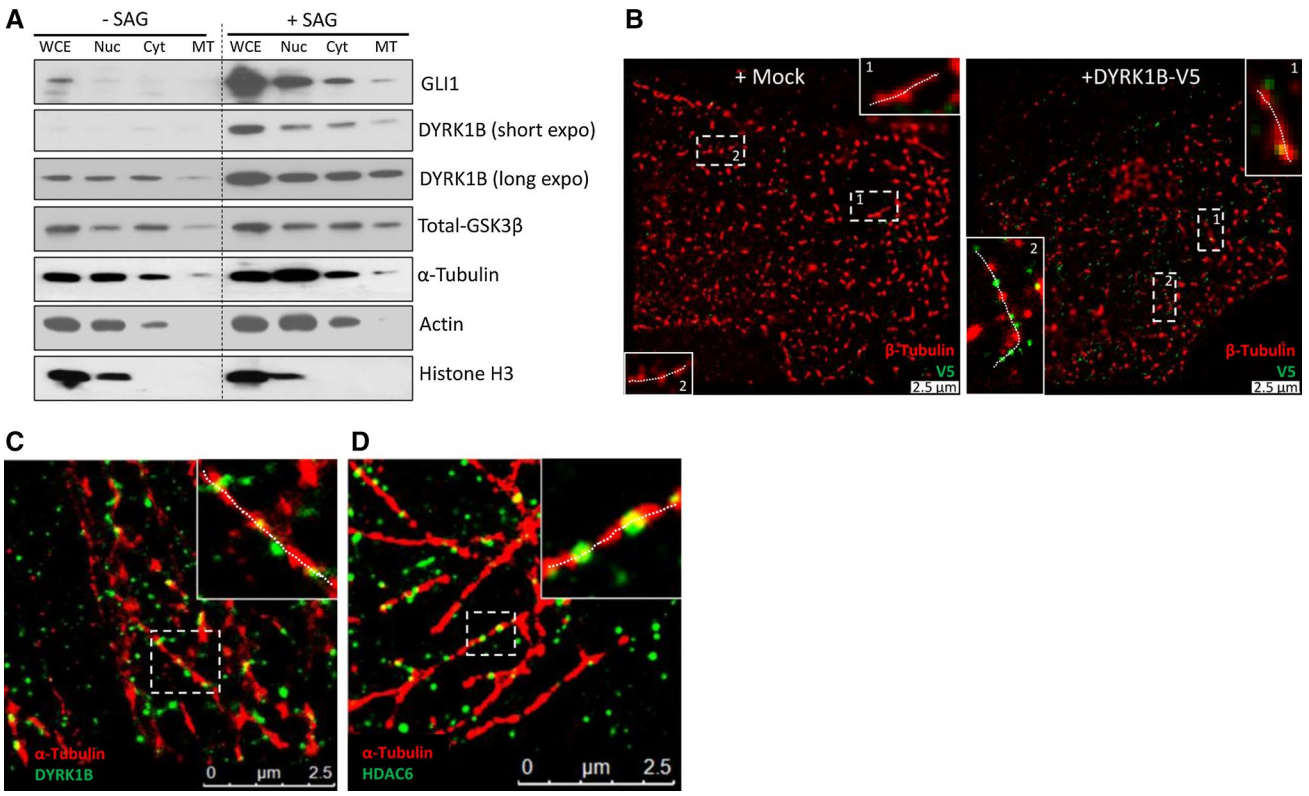

Fig. 4 DYRK1B is associated with microtubules. **a** Microtubule-association assay (MTaa) of lysates derived from control NIH3T3 cells or of cells treated with SAG (100 nM, 48 h). *WCE* whole cell extract, *Nuc* nuclear fraction, *Cyt* cytoplasmic fraction, *MT* polymerized MT-containing pellet. The levels of endogenous Hdac6 in control NIH3T3 cells were too low to be detected by Western blotting. Histone H3 (marker for nuclear fractions) and β-Actin was included to demonstrate purity of fractions. Shown is one representative experiment of $n=3$. **b** Super resolution images by means of ground state depletion (GSD) microscopy showing transiently transfected human PSC cells. Left panel: mock-transfected; right panel: DYRK1B-V5 transfected. Red = endogenous β-tubulin. Green = V5-antibody. The orientation of microtubules is indicated as faint white dotted lines in the insets. A scale bar of 2.5 µm is given. **c** GSD-image of non-transfected Hela cells. Red = endogenous α-tubulin. Green = endogenous DYRK1B. **d** GSD-image of non-transfected PSC cells. Red = endogenous α-tubulin. Green = endogenous HDAC6. The soluble cytoplasm has been washed out before in this experiment

Hh signaling enhances the intracellular transport of mitochondria

After having investigated mechanistic aspects of the Hh-DYRK1B-GSK3β-HDAC6-AcTub axis, we wanted to address the functional consequences of this chain of events. To this end, we investigated different cellular processes which have been described as being dependent on MTs and which are potentially influenced by MT-PTMs: Intracellular mitochondrial transport and mesenchymal cell polarization coupled with directed cell migration. First, we analyzed MT-dependent mitochondrial transport where tubulin acetylation had been shown to facilitate organelle motility in neurons [13]. To investigate whether Hh signaling affects mitochondrial transport, we generated NIH3T3 cells stably expressing fluorescent Dendra protein fused to a mitochondrial targeting sequence derived from human cytochrome c oxidase subunit 8a (NIH$^{[Cox8a\text{-}Dendra]}$ cells). The mitochondrial expression of this fusion protein was verified by its perfect co-localization with MitoTracker (Fig. 5a). In addition, we also verified the SAG- and Dyrk1b-dependent regulation of AcTub levels in these cells (Fig. 5b).

Using live cell imaging on the NIH$^{[Cox8a\text{-}Dendra]}$ cells, we first demonstrated that MT depolymerization by means of Nocodazole addition significantly reduced the overall distance (track length) and the speed of labelled mitochondria, verifying the importance of MT-dependent transport in this process (Fig. S4A, B). In addition, when we plotted the mean square displacement (MSD) rate as a quantitative measure for directionality [4], we observed a decreased directionality in mitochondrial transport, as would be expected in a situation in which the MT tracks have been destroyed (Fig. S4C).

Next, we investigated the impact of Hh activation (SAG), Dyrk1b inhibition (AZ191) and Hdac6 inhibition (ACY-1215 [66]) on mitochondrial transport. We decided to measure a longer time frame (3 h) than in the previous Nocodazole experiment, with less resolution to get an idea of physiologically meaningful intracellular distances (although

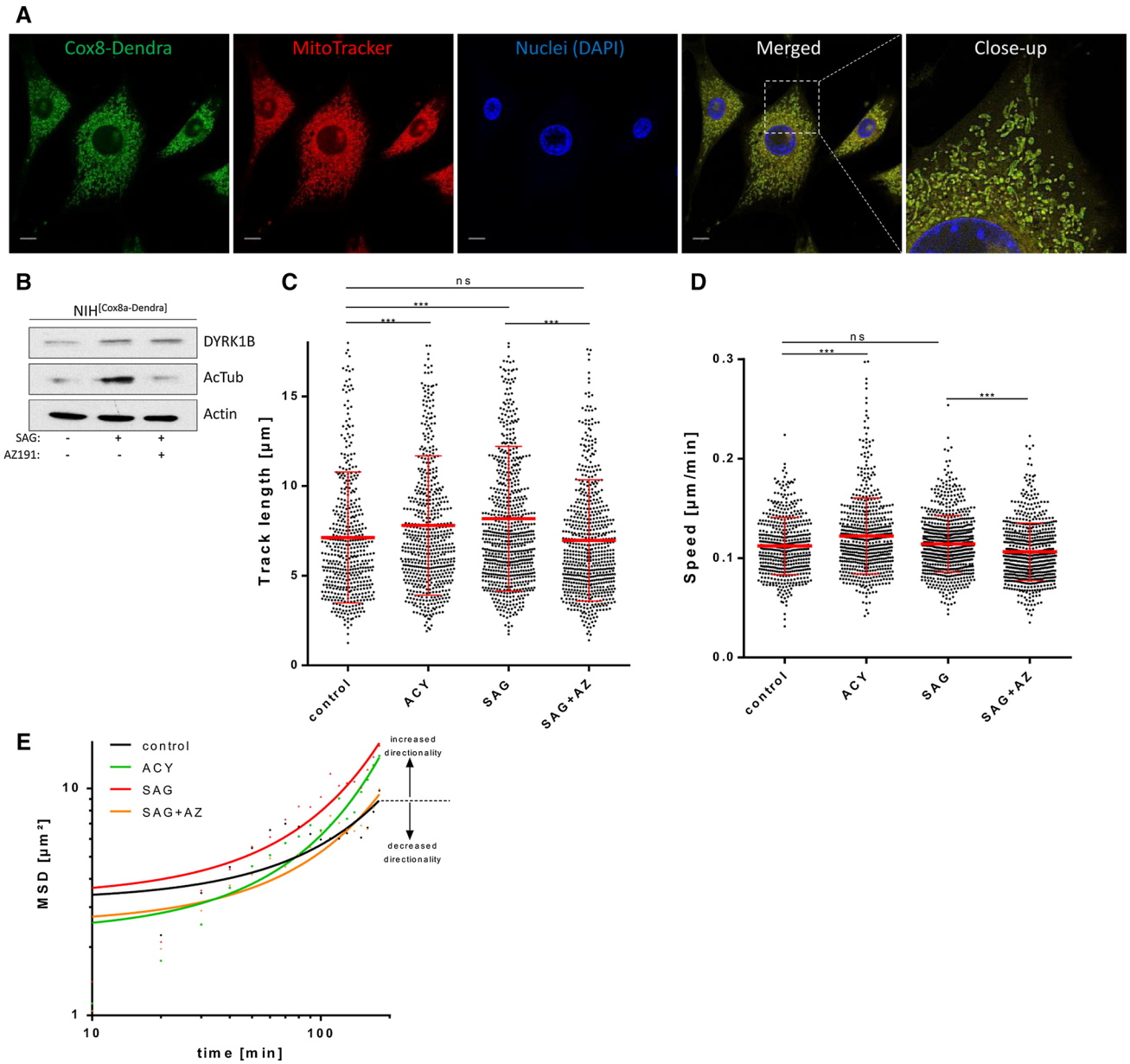

Fig. 5 Hh signaling facilitates organelle transport. **a** Confocal image of NIH3T3 cells stably expressing a *Cox8a-Dendra2* fusion construct (NIH[Cox8a-Dendra]; green). In addition, cells were co-stained with MitoTracker (red). Nuclei appear in blue. Scale bar represents 10 µm. **b** Levels of Dyrk1b and acetylated tubulin in SAG (100 nM, 48 h)- and AZ191 (DYRK1B inhibitor, 0.5 µM for last 2 h)-treated NIH[Cox8a-Dendra] cells. **c** Track length of mitochondria movement over a 3 h time window in NIH[Cox8a-Dendra] cells. Shown is one representative experiment (×20 objective) measuring three different cells of $n=4$ independent experiments. At least 500 events were recorded for each condition. Drug concentrations were: ACY-1215 (ACY, HDAC6 inhibitor) 10 µM; SAG 100 nM; AZ191 0.5 µM (all in 0.5%FBS). **d** Speed of mitochondria movement over a 3 h time window in NIH[Cox8a-Dendra] cells. Shown is one representative experiment (×20 objective) measuring three different cells of $n=4$ independent experiments. At least 500 events were recorded for each condition. Drug concentrations were: ACY-1215 (ACY) 10 µM; SAG 100 nM; AZ191 0.5 µM (all in 0.5% FBS). **e** Mean square displacement (MSD) over time. Shown is the MSD calculation (exponential curve fitting) of the experiment depicted in **c**, **d**. An increase in directed transport is reflected as an increased slope

this meant that we might not have recorded all short lateral movements). Nevertheless, our recordings clearly showed that when compared to untreated control cells, SAG stimulation significantly increased the overall track length of transported mitochondria (Fig. 5c). Importantly, this effect could be completely abrogated by co-application of the Dyrk1b antagonist AZ191 (Fig. 5c). In line with the hypothesized function of acetylated tubulin in organelle mobility,

the mere induction of AcTub levels by the small molecule Hdac6 inhibitor ACY-1215 also led to a significant increase in mitochondrial track length. In addition, also the mitochondrial transport speed was significantly increased by ACY-1215 and there was a trend towards increased speed with SAG application. Again, pharmacological blockade of Dyrk1b resulted in a clear reduction in mitochondria transport speed in SAG-treated cells (Fig. 5d). These conclusions could be verified by knocking down endogenous Dyrk1b which, as expected, negatively affected mitochondrial transport length and speed (Fig. S5D, S5E).

Plotting the MSD revealed that Hh signaling (SAG) increased the directed movement, whereas the co-application of AZ191 completely abrogated this surplus in directionality (Fig. 5e). Moreover, inducing tubulin acetylation by pharmacological Hdac6 inhibition (ACY-1215) also led to more directionality in mitochondrial transport, strongly suggesting that these effects are largely mediated through tubulin acetylation. In summary, we could provide evidence for Hh signaling enhancing MT-based intracellular organelle transport and for a critical role of Dyrk1b in this process.

Hh promotes cell polarization and directed migration through DYRK1B

In our attempts to link Hh signaling, DYRK1B and MT-PTMs to physiological events, we next turned to another MT-dependent process: The polarization of migrating mesenchymal cells, a process which can be recapitulated in in vitro wounding assays. In confluent cultures of fibroblasts, cells are usually not polarized towards a particular direction and the microtubule organizing center (MTOC) can be found randomly localized around the nucleus. However, if a scratch wound is applied to the cultured monolayer, cells at the border re-orient their MTOC towards the wound. This sequence of events requires, among others, inactive GSK3β and the MT-bound motor protein dynein [23, 26, 28, 45]. In addition, cell polarization and the subsequent directed cell migration toward the wound need the stabilization of MTs [28].

Therefore, we performed in vitro wounding assays in confluent fibroblast cultures and stained for the MTOC (using an α-pericentriolar material 1 (PCM-1) antibody) and the MT cytoskeleton (α-αTub antibody). As can be seen in Fig. 6a, b (and S6A), induction of Hh signaling by SAG led to an increase in cell polarization towards the wound. Increased cell polarization was also observed with the independent MT stabilizer ACY-1215 (Hdac6 inhibitor) (Fig. 6a, b). In line with our previous results on the involvement of Dyrk1b in AcTub regulation, we found that blocking Dyrk1b function with AZ191 abrogated the Hh-mediated mesenchymal cell polarization (Fig. 6c).

As the polarization of mesenchymal cells is the first step for directed migration into, e.g., wounded areas, we tested the impact of Dyrk1b inhibition on Hh-driven scratch wound closure using live cell imaging (Fig. 6d). As expected, when compared to control cells, SAG promoted the migration of NIH3T3 fibroblasts into an in vitro wound (Fig. 6e). When AZ191 was co-administered, this increase in migratory potential was blunted. Importantly, similar findings were made when endogenous DYRK1B was removed by genetic means using RNAi (Fig. S6B). These data demonstrate an important role for Dyrk1b in Hh-induced fibroblast polarization, cell motility and experimental wound closure.

Discussion

A considerable amount of data has been accumulated on the mechanisms of MT-dependent cellular processes such as intracellular transport and mitosis, but little knowledge exists on how extracellular ligands actually modulate cytoskeletal events. Here, we show that Hh signaling has the capability to affect MT acetylation and MT-dependent processes through induction of DYRK1B. In contrast to many other kinases, DYRKs are mainly regulated through their overall abundance. Even small changes in total DYRK amount can have significant impact on cellular functions, as evidenced for instance by the devastating contributing effects of the 1.5-fold increase in DYRK1A levels on neuronal and brain development in Down syndrome (Trisomy 21) patients [22]. As such, we anticipate that also moderate Hh-induced DYRK1B increases could have larger impact on cellular processes, such as tubulin acetylation. We are, however, also aware of the fact that highly complex processes such as cell migration involve numerous regulators on several cellular levels and that the posttranslational modification of tubulin most likely exerts a modifying role and is not the sole cause of these processes.

Nevertheless, *DYRK1B* has previously been identified as a potent promigratory gene in ovarian cancer cells [14], which often harbor a 19q13 chromosomal *DYRK1B*-containing amplicon or display elevated expression of this kinase by other means [24]. In addition, work in pancreatic cancer revealed that DYRK1B can protect cells from the MT-depolymerizing agent Nocodazole [17]. Our data provide a mechanistic explanation for these observations and present evidence for the role of this kinase in regulating MT acetylation. We find that a fraction of the cellular DYRK1B pool is localized to the microtubule cytoskeleton. Functionally, it inactivates GSK3β by direct phosphorylation of Ser9, leading to the indirect suppression of HDAC6 enzyme activity, a major cellular regulator of tubulin acetylation. Since both, GSK3β and HDAC6 can also associate to MTs, it is reasonable to speculate that these proteins form a functional unit

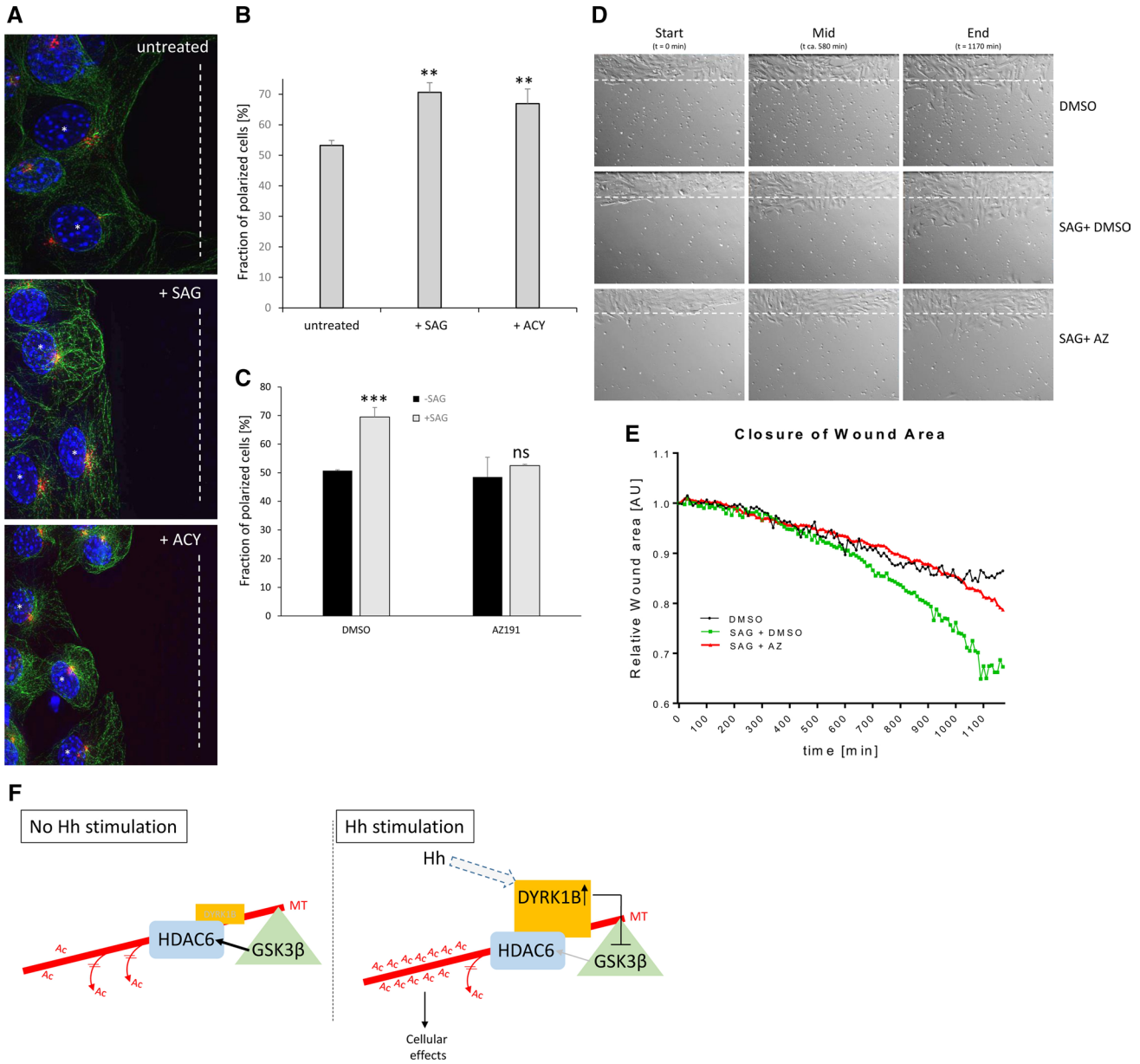

Fig. 6 Hedgehog promotes mesenchymal cell polarization and cell migration. **a** Microscopic determination of NIH3T3 fibroblast polarization by means of MTOC (PCM1, red) and α-tubulin (green) staining. Nuclei appear in blue. The orientation of the scratch is indicated by a white dashed line. Positive polarization towards the wound is indicated by a white asterisk. For experimental details see materials and methods section. **b** Quantification of the polarization experiment depicted in **e** (mean of $n = 3 \pm$ SD). SAG (SMO agonist, 100 nM); ACY-1215 (HDAC6 inhibitor, 10 µM). **c** Fraction of polarized NIH3T3 fibroblasts, pre-treated with SAG (100 nM) for 2d, followed by scratch wounding. DMSO or AZ191 (Dyrk1b inhibitor, 0.5 µM) was added 30 min before the scratch. Shown is the mean of $n = 3 \pm$ SD. **d** Example of scratch wounds in confluent NIH3T3 cultures directly after scratching (Start, left), after approx. 9.5 h (Mid, middle) or at the end (approx. 20 h, right panel). The border is outlined by a dashed line. AZ = AZ191 (1 µM). **e** Relative wound closure over time as assessed by live cell recording. One representative example of three is shown. AZ = AZ191 (1 µM). **f** Schematic depiction of the findings described in this manuscript. Left panel: Without Hh stimulation. Right panel: With Hh stimulation. Not shown is the possibility that Hh/SMO might also activate AKT, leading to an additional route of GSK3β regulation. DYRK1B can also functionally interact with AKT

at or around MTs (Fig. 6f). The elucidation of how exactly HDAC6 is regulated by GSK3β awaits further studies. Moreover, additional HDAC6 regulators are known [82] and we cannot fully rule out that modulators other than GSK3β also play a currently unidentified role in Hh-mediated regulation of tubulin acetylation.

Of note, we have previously shown that DYRK1B is able to manipulate PI3K/AKT signaling, which itself is

subject to intense feedback control mechanisms [72]. As AKT can potentially phosphorylate GSK3β independently of DYRK1B, this complex network of signaling molecules could complicate the predictability of the net effect of tubulin acetylation, particularly at time points at which feedback mechanism are still at play. Adding to this situation are somatic mutations activating the PI3K/AKT kinase arm in a constitutive manner as found in many cancer cells.

Supporting and extending previously published evidence on Hh-regulated tubulin regulation [42], our manuscript integrates this regulation into a wider mechanistic framework ranging from Hh ligands to modulation of intracellular cytoskeletal outputs. In this respect, it is interesting to note that both Hh signaling as well as HDAC6 inhibition/MT acetylation were found to drive Interleukin-10 production [43, 79]. Furthermore, DYRK1B and HDAC6 seem to be regulatory components of the Hh cascade itself, raising the possibility for cytoskeleton-mediated autoregulation of the pathway [20, 29, 41]. If and to what extent acetylation-dependent transport processes along ciliary and non-ciliary MTs modulate canonical Hh signaling awaits further investigation.

Our results of Hh-mediated MT control through effects on tubulin PTMs, and not through effects on, e.g., motor proteins, add a new layer of complexity to the regulation of directed cell migration, a process involving a large number of proteins. Whether these effects utilize the canonical Hh signaling cascade or whether other 'non-canonical' mechanisms are responsible requires further studies. Certain non-canonical mechanisms at several levels have been reported to modulate Hh-induced cell migration, such as non-ciliary SMO and/or GLI-independent regulation of the actin cytoskeleton [6, 7, 56, 57].

Another interesting finding of this study is the fact that Hh signaling promotes the transport of mitochondria along MTs in non-neuronal cells such as fibroblasts. Until now, MT-based mitochondrial motility has been mostly investigated in neuronal cells, where long axons necessitate the transport of mitochondria to distant sites for local ATP production [68]. However, there is emerging evidence that the subcellular localization of mitochondria is also important for cell migration in non-neuronal cells [19]. In addition, the first links between mitochondrial dynamics and cellular metabolism are considered [52]. In light of the fact that *DYRK1B* has recently been associated with the metabolic syndrome [31, 38], a potential role of mitochondria will be interesting to follow up. Furthermore, Hh signaling has been implicated in controlling the functionality of the T cell immunological synapse, a structure relying, among others, on motor protein driven mitochondrial transport [16, 60].

In summary, we present a mechanistic framework how extracellular Hh ligands can modulate the PTM status of MTs and can subsequently contribute to the regulation of intracellular MT-dependent processes such as cell polarization, migration and organelle transport.

Materials and methods

Cell lines

NIH3T3 and HeLa cell lines were purchased from ATCC. MEF and MEF$^{[SHH]}$ cells were kindly provided by Wade Bushman [47]. PSC cells were a kind gift of M. Löhr [36]. The generation of NIH3T3 cells stably expressing empty vector control or *DYRK1B* was described in [72]. All cell lines were mycoplasma-free and were cultured in Dulbecco's Modified Eagle Medium (DMEM (high Glucose plus Glutamine and Pyruvate), Invitrogen) supplemented with 10% fetal bovine serum (FBS) and 1% penicillin/streptomycin at 37 °C with 5% CO_2. If not otherwise stated, serum concentrations were reduced to 0.5% during experiments for all cell types.

Plasmid transfection

NIH3T3 cells were transfected with TransIT-2020 (Mirus Bio) according to the manufacturer's protocol. The following plasmids were employed: EF1α-promoter driven DYRK1B and kinase-dead DYRK1B$^{Y271F/Y273F}$ (DYRK1B(YF)) expression constructs [72]; H2B-mCherry (Addgene #20972) [54]; dominant active GSK3β^{S9A} (Addgene #14754) [74].

Small-interfering RNA (siRNA) transfection

Cells were transfected with 35 nM siRNA (Dharmacon SMARTpools and Qiagen control siRNA using RNAiMax (Invitrogen). Control siRNA (siCon) was purchased from Qiagen (All-Stars-siRNA; siAll). The mouse *Dyrk1b*-specific siRNA was an equimolar pool of four target sequences: si1b_1: AUACAGAGAUGAAGUACUA; si1b_2: GCACAUCAAUGAGGUAUAC; si1b_3: GAGAUGAAGUACUACAUAG; si1b_4: GGACAAAG*GAACUCAGGAA*. The human *DYRK1B*-specific siRNA target sequences were: si1B_3: GAGAUGAAGUACUAUAUAG; si1B_4: CGAAAGAACUCAGGAAGGA; si1B_5: GGUGAAAGCCUAUGAUCAU; si1B_6: GGACCUACCGCUACAGCAA.

RNA preparation, cDNA synthesis, qPCR

Total RNA was extracted using NucleoSpin RNA II kit (Macherey–Nagel) according to the manufacturer's protocol. cDNA synthesis of 1 µg total RNA was performed using iScript cDNA Synthesis Kit (Biorad) following the manufacturer's guidelines. Quantitative PCR reactions

were performed using the Absolute QPCR SYBR Green Mix (ABGene). qPCR reactions were performed on 96 well qPCR plates (ABGene) using either the Mx3000P or Mx3005P qPCR systems (Agilent). Results were calculated as relative mRNA expression ($2^{\Delta\Delta Ct}$). Data were obtained from at least three independent experiments and is shown as the mean ± SD. Primer sequences (5′ to 3′) for the detection of mouse *Dyrk1b* were: For-TTGACACCTGCCCCT CCTCTAGCAC; Rev-GGCCCCCACAATATCGGTTGC TGTA. Human *DYRK1B*: For-TTGGCCAGGTGGTGA AAGCCTATGA; Rev-CAATCTGGGCCTGGTTCAGGA AAGC. Mouse *Hdac6*: For-TCCCTACAGCTTGGGGTT CTCAGCA; Rev-TCCCCAAATCCTTGTGTCAGCATC A. Mouse *Mec17*: For-TGACCGGGAGGCTCACAATGA GGTA; Rev-TGGGGCTCCACTCGCTCTTTCTGTA. All other primer sequences have been described elsewhere [20, 69, 76, 77].

Western blotting

Separation of lysates by SDS-PAGE was followed by subsequent Western Blot analysis. SDS-PAGE gels were blotted on Immobilon-PVDF membranes (Millipore) and incubated with the respective primary antibody, followed by an HRP-coupled secondary antibody. Detection of the HRP signal was performed using Pierce ECL Western Blotting Substrate (Thermo Fisher Scientific, Waltham, USA) according to the manufacturer's protocol. The following primary antibodies were used: α-DYRK1A (#2771; Cell Signaling Technology (CST), Danvers, USA); α-DYRK1B (#5672; CST); α-DYRK2 (#8143; CST); α-DYRK3 (sc-390532; Santa Cruz Biotechnology, Santa Cruz, USA); α-GLI1 (#2643; CST); α-phospho-GSK3β^{S9} (#5558, CST); α-total GSK3β (#12456, CST); α-acetylated α-tubulin (AcTub, T6793, Sigma-Aldrich, St. Louis, USA); α-tyrosinated-α-tubulin; α-polyglutamylated-α/β-tubulin; α-α-tubulin (T6199, Sigma); α-Histone H3 (#39163, Active Motif); α-GAPDH (#G9545; Sigma); α-β-Actin (#A5441; Sigma).

Immunofluorescence on fixed samples

Cells were seeded on cover slips and fixed with 4% formaldehyde/PBS for 10 min at RT. After washing twice with PBS at RT for 5 min, cells were permeabilized with 0.5% Triton-X100/PBS at RT for 5 min. For immunostaining, cover slips were blocked with 10% serum/PBS for 1 h at RT and washed with PBS at RT for 10 min. Primary antibody α-acetylated α-tubulin (Sigma, T6793, clone 6-11B-1, 1:1000) was diluted in PBS containing 10% serum and 0.1% saponin and incubated overnight at 4 °C. After washing twice with PBS at RT for 5 min, the cover slips were incubated with fluorophor-coupled secondary antibodies diluted in PBS containing 10% serum and 0.1% saponin at RT in the dark for 2 h. After washing twice with PBS for 5 min and rinsing with H_2O, the cells were covered with mounting medium containing DAPI. Microscopy was performed on a Leica DMR epifluorescence and a Leica AF6000 widefield fluorescence microscope with 3D deconvolution software (Leica Microsystems, Wetzlar, Germany).

Microtubule-association assay (MTaa)

Fully confluent NIH3T3 fibroblasts were incubated on 10-cm culture dishes in 0.5% FBS-containing DMEM with or without SAG (100 nM) for 48 h. Subsequently, cells were washed with warm PBS, scraped off and pelleted (300*g*, 30 s, RT), followed by resuspension in PBS/Taxol (20 µM) and incubation for 15 min at RT. After another centrifugation step (300*g*, 30 s, RT), cells were resuspended in 1 ml of room temperature MTaa lysis buffer (1 mM EGTA, 0.05% NP-40, 3 mM $MgCl_2$, 100 mM NaCl, 10 mM Tris pH 7.5 plus protease inhibitors) and an aliquot (400 µl) of the lysate was stored (whole cell lysate). The remaining cell lysate (600 µl) was layered on a cushion of cold MTaa lysis buffer containing 1 M sucrose and centrifuged (400*g*, 5 min, RT) to pellet the nuclear fraction. The supernatant was transferred to a new tube for ultracentrifugation (27,000*g*, 45 min, RT) to pellet unwanted membrane debri. The supernatant was collected and another ultracentrifugation step was performed (100,000*g*, 90 min, RT). The supernatant collected from this step was stored as cytoplasmic fraction and the pellet was taken as polymerized microtubule fraction.

Cell polarization assay

NIH3T3 cells were grown confluent on glass cover slips (24 h) followed by another 24 h in the presence of 100 nM SAG (0.5% FBS). Subsequently, DMSO, ACY1215 (10 µM) or AZ191 (0.5 µM) was added for 30 min followed by wounding of the confluent monolayer with a yellow pipette tip. Cells were washed once with medium, followed by addition of 3% FBS-containing medium containing SAG/DMSO/ACY-1215/AZ191 for 6 h at 37° C. Cells were fixed with 3.7% formaldehyde, stained with antibodies against α-tubulin and pericentriolar material 1 (PCM1) and mounted in Vectashield containing DAPI (Vectorlabs). Images shown in the manuscript are maximum intensity projections of 3D-deconvoluted Z-stacks taken on a Leica AF6000 widefield fluorescence microscope with 3D deconvolution software.

Ground state depletion microscopy (GSD)

GSD was performed on a Leica GSDIM Super Resolution SR microscope system according to the manufacturer's protocols using AlexaFluor488- and AlexaFluor647-labelled

secondary antibodies. In some cases, the soluble cytoplasm was washed out before fixation by gently shaking the cells for 2 × 5 min in 1 M EGTA/2.5 mM GTP/4% PEG-6000/0.1 M PIPES/0.2% Triton-X100 at room temperature.

Live cell measurement of mitochondrial transport

Cells were grown in chamber slides (Ibidi) in 0.5% FBS for 48 h with/without SAG (100 nM), followed by addition of DMSO, ACY-1215 (10 µM) or AZ191 (0.5 µM). Live cell imaging was started approx. 30 min later. Recordings were taken on a laser scanning confocal microscope (LSCM) (Leica TCS-SP8i) with an incubation chamber tempered to 37 °C. Recordings were made in 10 min intervals from several slide areas for a duration of 3 h (20× objective, NA 0.75, 1024 × 1024 pixel, 2× average, zoom 3.0). Analysis of mitochondria motility from three cells was done in Imaris software (Bitplane, v8.2.0) using the spot algorithm. The overall movement of the cells was set to zero using the surface algorithm before mitochondria calculations.

Statistical analysis

Unless otherwise stated, data are presented as the mean of three independent experiments ± standard deviation (SD). Statistical significance was calculated by applying a two-tailed Student's *t* test. $*p < 0.05$; $**p < 0.01$; $***p < 0.001$.

Acknowledgements This work was supported by grants obtained from the German Research Society (DFG-KFO325 and DFG-LA2829/9-1), the Behring-Röntgen Foundation and the University Hospital Giessen-Marburg (UKGM).

Compliance with ethical standards

Conflict of interest No competing interest declared.

References

1. Aberger F, Ruiz IAA (2014) Context-dependent signal integration by the GLI code: the oncogenic load, pathways, modifiers and implications for cancer therapy. Semin Cell Dev Biol 33:93–104
2. Akella JS, Wloga D, Kim J, Starostina NG, Lyons-Abbott S, Morrissette NS, Dougan ST, Kipreos ET, Gaertig J (2010) MEC-17 is an alpha-tubulin acetyltransferase. Nature 467:218–222
3. Ashford AL, Oxley D, Kettle J, Hudson K, Guichard S, Cook SJ, Lochhead PA (2014) A novel DYRK1B inhibitor AZ191 demonstrates that DYRK1B acts independently of GSK3beta to phosphorylate cyclin D1 at Thr(286), not Thr(288). Biochem J 457:43–56
4. Bacher CP, Reichenzeller M, Athale C, Herrmann H, Eils R (2004) 4-D single particle tracking of synthetic and proteinaceous microspheres reveals preferential movement of nuclear particles along chromatin—poor tracks. BMC Cell Biol 5:45
5. Barakat MT, Humke EW, Scott MP (2010) Learning from Jekyll to control Hyde: Hedgehog signaling in development and cancer. Trends Mol Med 16:337–348
6. Bijlsma MF, Borensztajn KS, Roelink H, Peppelenbosch MP, Spek CA (2007) Sonic hedgehog induces transcription-independent cytoskeletal rearrangement and migration regulated by arachidonate metabolites. Cell Signal 19:2596–2604
7. Bijlsma MF, Damhofer H, Roelink H (2012) Hedgehog-stimulated chemotaxis is mediated by smoothened located outside the primary cilium. Sci Signal 5:ra60
8. Boyault C, Zhang Y, Fritah S, Caron C, Gilquin B, Kwon SH, Garrido C, Yao TP, Vourc'h C, Matthias P et al (2007) HDAC6 controls major cell response pathways to cytotoxic accumulation of protein aggregates. Genes Dev 21:2172–2181
9. Briscoe J, Therond PP (2013) The mechanisms of Hedgehog signalling and its roles in development and disease. Nat Rev Mol Cell Biol 14:416–429
10. Cai D, McEwen DP, Martens JR, Meyhofer E, Verhey KJ (2009) Single molecule imaging reveals differences in microtubule track selection between Kinesin motors. PLoS Biol 7:e1000216
11. Chen JK, Taipale J, Young KE, Maiti T, Beachy PA (2002) Small molecule modulation of Smoothened activity. Proc Natl Acad Sci USA 99:14071–14076
12. Chen PB, Hung JH, Hickman TL, Coles AH, Carey JF, Weng Z, Chu F, Fazzio TG (2013) Hdac6 regulates Tip60-p400 function in stem cells. Elife 2:e01557
13. Chen S, Owens GC, Makarenkova H, Edelman DB (2010) HDAC6 regulates mitochondrial transport in hippocampal neurons. PLoS One 5:e10848
14. Collins CS, Hong J, Sapinoso L, Zhou Y, Liu Z, Micklash K, Schultz PG, Hampton GM (2006) A small interfering RNA screen for modulators of tumor cell motility identifies MAP4K4 as a promigratory kinase. Proc Natl Acad Sci US A 103:3775–3780
15. Dafinger C, Liebau MC, Elsayed SM, Hellenbroich Y, Boltshauser E, Korenke GC, Fabretti F, Janecke AR, Ebermann I, Nurnberg G et al (2011) Mutations in KIF7 link Joubert syndrome with Sonic Hedgehog signaling and microtubule dynamics. J Clin Invest 121:2662–2667
16. de la Roche M, Ritter AT, Angus KL, Dinsmore C, Earnshaw CH, Reiter JF, Griffiths GM (2013) Hedgehog signaling controls T cell killing at the immunological synapse. Science 342:1247–1250
17. Deng X, Ewton DZ, Li S, Naqvi A, Mercer SE, Landas S, Friedman E (2006) The kinase Mirk/Dyrk1B mediates cell survival in pancreatic ductal adenocarcinoma. Cancer Res 66:4149–4158
18. Deribe YL, Wild P, Chandrashaker A, Curak J, Schmidt MH, Kalaidzidis Y, Milutinovic N, Kratchmarova I, Buerkle L, Fetchko MJ et al (2009) Regulation of epidermal growth factor receptor trafficking by lysine deacetylase HDAC6. Sci Signal 2:ra84
19. Desai SP, Bhatia SN, Toner M, Irimia D (2013) Mitochondrial localization and the persistent migration of epithelial cancer cells. Biophys J 104:2077–2088
20. Dhanyamraju PK, Holz PS, Finkernagel F, Fendrich V, Lauth M (2014). Histone deacetylase 6 represents a novel drug target in the oncogenic Hedgehog signaling pathway. Mol Cancer Ther 14(3):727–39
21. Dompierre JP, Godin JD, Charrin BC, Cordelieres FP, King SJ, Humbert S, Saudou F (2007) Histone deacetylase 6 inhibition compensates for the transport deficit in Huntington's disease by increasing tubulin acetylation. J Neurosci 27:3571–3583
22. Duchon A, Herault Y (2016) DYRK1A, a dosage-sensitive gene involved in neurodevelopmental disorders, is a target for drug development in Down syndrome. Front Behav Neurosci 10:104
23. Etienne-Manneville S, Hall A (2003) Cdc42 regulates GSK-3beta and adenomatous polyposis coli to control cell polarity. Nature 421:753–756

24. Friedman E (2013) Mirk/dyrk1B kinase in ovarian cancer. Int J Mol Sci 14:5560–5575
25. Goetz SC, Anderson KV (2010) The primary cilium: a signalling centre during vertebrate development. Nat Rev Genet 11:331–344
26. Gomes ER, Jani S, Gundersen GG (2005) Nuclear movement regulated by Cdc42, MRCK, myosin, and actin flow establishes MTOC polarization in migrating cells. Cell 121:451–463
27. Gorojankina T (2016) Hedgehog signaling pathway: a novel model and molecular mechanisms of signal transduction. Cell Mol Life Sci 73(7):1317–32
28. Goulimari P, Knieling H, Engel U, Grosse R (2008) LARG and mDia1 link Galpha12/13 to cell polarity and microtubule dynamics. Mol Biol Cell 19:30–40
29. Gruber W, Hutzinger M, Elmer DP, Parigger T, Sternberg C, Cegielkowski L, Zaja M, Leban J, Michel S, Hamm S et al (2016) DYRK1B as therapeutic target in Hedgehog/GLI-dependent cancer cells with Smoothened inhibitor resistance. Oncotarget 7:7134–7148
30. Hammond JW, Huang CF, Kaech S, Jacobson C, Banker G, Verhey KJ (2010) Posttranslational modifications of tubulin and the polarized transport of kinesin-1 in neurons. Mol Biol Cell 21:572–583
31. Hickmott J (2015) DYRK1B variant linked to autosomal dominant metabolic syndrome. Clin Genet 87:30–31
32. Hubbert C, Guardiola A, Shao R, Kawaguchi Y, Ito A, Nixon A, Yoshida M, Wang XF, Yao TP (2002) HDAC6 is a microtubule-associated deacetylase. Nature 417:455–458
33. Hui CC, Angers S (2011) Gli proteins in development and disease. Annu Rev Cell Dev Biol 27:513–537
34. Janke C (2014) The tubulin code: molecular components, readout mechanisms, and functions. J Cell Biol 206:461–472
35. Janke C, Montagnac G (2017) Causes and consequences of microtubule acetylation. Curr Biol 27:R1287–R1292
36. Jesnowski R, Furst D, Ringel J, Chen Y, Schrodel A, Kleeff J, Kolb A, Schareck WD, Lohr M (2005) Immortalization of pancreatic stellate cells as an in vitro model of pancreatic fibrosis: deactivation is induced by matrigel and *N*-acetylcysteine. Lab Invest 85:1276–1291
37. Kawaguchi Y, Kovacs JJ, McLaurin A, Vance JM, Ito A, Yao TP (2003) The deacetylase HDAC6 regulates aggresome formation and cell viability in response to misfolded protein stress. Cell 115:727–738
38. Keramati AR, Fathzadeh M, Go GW, Singh R, Choi M, Faramarzi S, Mane S, Kasaei M, Sarajzadeh-Fard K, Hwa J et al (2014) A form of the metabolic syndrome associated with mutations in DYRK1B. N Engl J Med 370:1909–1919
39. Khatra H, Khan PP, Pattanayak S, Bhadra J, Rather B, Chakrabarti S, Saha T, Sinha S (2018) Hedgehog antagonist pyrimidine-indole hybrid molecule inhibits ciliogenesis through microtubule destabilisation. ChemBioChem 19:723–735
40. Kwon S, Zhang Y, Matthias P (2007) The deacetylase HDAC6 is a novel critical component of stress granules involved in the stress response. Genes Dev 21:3381–3394
41. Lauth M, Bergstrom A, Shimokawa T, Tostar U, Jin Q, Fendrich V, Guerra C, Barbacid M, Toftgard R (2010) DYRK1B-dependent autocrine-to-paracrine shift of Hedgehog signaling by mutant RAS. Nat Struct Mol Biol 17:718–725
42. Lee H, Ko HW (2016) Ciliary smoothened-mediated noncanonical hedgehog signaling promotes tubulin acetylation. Biochem Biophys Res Commun 480:574–579
43. Lee JJ, Rothenberg ME, Seeley ES, Zimdahl B, Kawano S, Lu WJ, Shin K, Sakata-Kato T, Chen JK, Diehn M et al (2016a). Control of inflammation by stromal Hedgehog pathway activation restrains colitis. Proc Natl Acad Sci USA
44. Lee RT, Zhao Z, Ingham PW (2016) Hedgehog signalling. Development 143:367–372
45. Li R, Gundersen GG (2008) Beyond polymer polarity: how the cytoskeleton builds a polarized cell. Nat Rev Mol Cell Biol 9:860–873
46. Li Y, Shin D, Kwon SH (2012) Histone deacetylase 6 plays a role as a distinct regulator of diverse cellular processes. FEBS J 280(3):775–93
47. Lipinski RJ, Bijlsma MF, Gipp JJ, Podhaizer DJ, Bushman W (2008) Establishment and characterization of immortalized Gli-null mouse embryonic fibroblast cell lines. BMC Cell Biol 9:49
48. Magiera MM, Singh P, Gadadhar S, Janke C (2018) Tubulin posttranslational modifications and emerging links to human disease. Cell 173:1323–1327
49. Mak AB, Nixon AM, Kittanakom S, Stewart JM, Chen GI, Curak J, Gingras AC, Mazitschek R, Neel BG, Stagljar I et al (2012) Regulation of CD133 by HDAC6 promotes beta-catenin signaling to suppress cancer cell differentiation. Cell Rep 2:951–963
50. McGlinn E, Tabin CJ (2006) Mechanistic insight into how Shh patterns the vertebrate limb. Curr Opin Genet Dev 16:426–432
51. Mercer SE, Friedman E (2006) Mirk/Dyrk1B: a multifunctional dual-specificity kinase involved in growth arrest, differentiation, and cell survival. Cell Biochem Biophys 45:303–315
52. Mishra P, Chan DC (2016) Metabolic regulation of mitochondrial dynamics. J Cell Biol 212:379–387
53. Montagnac G, Meas-Yedid V, Irondelle M, Castro-Castro A, Franco M, Shida T, Nachury MV, Benmerah A, Olivo-Marin JC, Chavrier P (2013) alphaTAT1 catalyses microtubule acetylation at clathrin-coated pits. Nature 502:567–570
54. Nam HS, Benezra R (2009) High levels of Id1 expression define B1 type adult neural stem cells. Cell Stem Cell 5:515–526
55. Pak E, Segal RA (2016) Hedgehog signal transduction: key players, oncogenic drivers, and cancer therapy. Dev Cell 38:333–344
56. Polizio AH, Chinchilla P, Chen X, Kim S, Manning DR, Riobo NA (2011) Heterotrimeric Gi proteins link Hedgehog signaling to activation of Rho small GTPases to promote fibroblast migration. J Biol Chem 286:19589–19596
57. Polizio AH, Chinchilla P, Chen X, Manning DR, Riobo NA (2011b) Sonic Hedgehog activates the GTPases Rac1 and RhoA in a Gli-independent manner through coupling of smoothened to Gi proteins. Sci Signal 4:pt7
58. Portran D, Schaedel L, Xu Z, Thery M, Nachury MV (2017) Tubulin acetylation protects long-lived microtubules against mechanical ageing. Nat Cell Biol 19:391–398
59. Pugacheva EN, Jablonski SA, Hartman TR, Henske EP, Golemis EA (2007) HEF1-dependent Aurora A activation induces disassembly of the primary cilium. Cell 129:1351–1363
60. Quintana A, Hoth M (2012) Mitochondrial dynamics and their impact on T cell function. Cell Calcium 52:57–63
61. Reed NA, Cai D, Blasius TL, Jih GT, Meyhofer E, Gaertig J, Verhey KJ (2006) Microtubule acetylation promotes kinesin-1 binding and transport. Curr Biol 16:2166–2172
62. Reiter JF, Leroux MR (2017) Genes and molecular pathways underpinning ciliopathies. Nat Rev Mol Cell Biol 18:533–547
63. Robbins DJ, Fei DL, Riobo NA (2012) The hedgehog signal transduction network. Sci Signal 5:re6
64. Rohatgi R, Milenkovic L, Scott MP (2007) Patched1 regulates hedgehog signaling at the primary cilium. Science 317:372–376
65. Sakai N, Tager AM (2013) Fibrosis of two: epithelial cell-fibroblast interactions in pulmonary fibrosis. Biochim Biophys Acta 1832:911–921
66. Santo L, Hideshima T, Kung AL, Tseng JC, Tamang D, Yang M, Jarpe M, van Duzer JH, Mazitschek R, Ogier WC et al (2012) Preclinical activity, pharmacodynamic, and pharmacokinetic properties of a selective HDAC6 inhibitor, ACY-1215, in combination with bortezomib in multiple myeloma. Blood 119:2579–2589

67. Sasaki N, Kurisu J, Kengaku M (2010) Sonic hedgehog signaling regulates actin cytoskeleton via Tiam1-Rac1 cascade during spine formation. Mol Cell Neurosci 45(4):335-44
68. Saxton WM, Hollenbeck PJ (2012) The axonal transport of mitochondria. J Cell Sci 125:2095–2104
69. Schneider P, Miguel Bayo-Fina J, Singh R, Kumar Dhanyamraju P, Holz P, Baier A, Fendrich V, Ramaswamy A, Baumeister S, Martinez ED et al (2015) Identification of a novel actin-dependent signal transducing module allows for the targeted degradation of GLI1. Nat Commun 6:8023
70. Shan B, Yao TP, Nguyen HT, Zhuo Y, Levy DR, Klingsberg RC, Tao H, Palmer ML, Holder KN, Lasky JA (2008) Requirement of HDAC6 for transforming growth factor-beta1-induced epithelial-mesenchymal transition. J Biol Chem 283:21065–21073
71. Shin K, Lee J, Guo N, Kim J, Lim A, Qu L, Mysorekar IU, Beachy PA (2011) Hedgehog/Wnt feedback supports regenerative proliferation of epithelial stem cells in bladder. Nature 472:110–114
72. Singh R, Dhanyamraju PK, Lauth M (2017) DYRK1B blocks canonical and promotes non-canonical Hedgehog signaling through activation of the mTOR/AKT pathway. Oncotarget 8:833–845
73. Song WJ, Song EA, Jung MS, Choi SH, Baik HH, Jin BK, Kim JH, Chung SH (2015) Phosphorylation and inactivation of glycogen synthase kinase 3beta (GSK3beta) by dual-specificity tyrosine phosphorylation-regulated kinase 1A (Dyrk1A). J Biol Chem 290:2321–2333
74. Stambolic V, Woodgett JR (1994) Mitogen inactivation of glycogen synthase kinase-3 beta in intact cells via serine 9 phosphorylation. Biochem J 303(Pt 3):701–704
75. Sun W, Qureshi HY, Cafferty PW, Sobue K, Agarwal-Mawal A, Neufield KD, Paudel HK (2002) Glycogen synthase kinase-3beta is complexed with tau protein in brain microtubules. J Biol Chem 277:11933–11940
76. Tariki M, Dhanyamraju PK, Fendrich V, Borggrefe T, Feldmann G, Lauth M (2014) The Yes-associated protein controls the cell density regulation of Hedgehog signaling. Oncogenesis 3:e112
77. Tariki M, Wieczorek SA, Schneider P, Banfer S, Veitinger S, Jacob R, Fendrich V, Lauth M (2013) RIO kinase 3 acts as a SUFU-dependent positive regulator of Hedgehog signaling. Cell Signal 25:2668–2675
78. Walter WJ, Beranek V, Fischermeier E, Diez S (2012) Tubulin acetylation alone does not affect kinesin-1 velocity and run length in vitro. PLoS ONE 7:e42218
79. Wang B, Rao YH, Inoue M, Hao R, Lai CH, Chen D, McDonald SL, Choi MC, Wang Q, Shinohara ML et al (2014) Microtubule acetylation amplifies p38 kinase signalling and anti-inflammatory IL-10 production. Nat Commun 5:3479
80. Westermann S, Weber K (2003) Posttranslational modifications regulate microtubule function. Nat Rev Mol Cell Biol 4:938–947
81. Xu Z, Schaedel L, Portran D, Aguilar A, Gaillard J, Marinkovich MP, Thery M, Nachury MV (2017) Microtubules acquire resistance from mechanical breakage through intralumenal acetylation. Science 356:328–332
82. Yan J (2014) Interplay between HDAC6 and its interacting partners: essential roles in the aggresome-autophagy pathway and neurodegenerative diseases. DNA Cell Biol 33:567–580
83. Zhang Y, Kwon S, Yamaguchi T, Cubizolles F, Rousseaux S, Kneissel M, Cao C, Li N, Cheng HL, Chua K et al (2008) Mice lacking histone deacetylase 6 have hyperacetylated tubulin but are viable and develop normally. Mol Cell Biol 28:1688–1701
84. Zilberman Y, Ballestrem C, Carramusa L, Mazitschek R, Khochbin S, Bershadsky A (2009) Regulation of microtubule dynamics by inhibition of the tubulin deacetylase HDAC6. J Cell Sci 122:3531–3541